GaN based transfer electron and avalanche transit time devices*

R. K. Parida[1] and A. K. Panda[2, †]

[1]ITER, Siksha 'O' Anusandhan University, Bhubaneswar, Odisha, 751030, India
[2]National Institute of Science and Technology, Palur Hills, Berhampur, Odisha, 761008, India

Abstract: A new model is developed to study the microwave/mm wave characteristics of two-terminal GaN-based transfer electron devices (TEDs), namely a Gunn diode and an impact avalanche transit time (IMPATT) device. Microwave characteristics such as device efficiency and the microwave power generated are computed and compared at D-band (140 GHz center frequency) to see the potentiality of each device under the same operating conditions. It is seen that GaN-based IMPATT devices surpass the Gunn diode in the said frequency region.

Key words: GaN; transfer electron device; avalanche transit time device
DOI: 10.1088/1674-4926/33/5/054001 **EEACC:** 2520

1. Introduction

The development of several solid state devices in recent years has helped to realize efficient communication systems involving a wide range of operating frequencies[1−5]. Solid state devices provide stable, cheap and reliable RF power even at very high operating frequencies, i.e. microwaves and mm-waves. Microwave devices are categorized as two and three terminal devices. Up till now, two-terminal devices have dominated over three-terminal devices in the high frequency region, particularly at 94 GHz and beyond[6]. Further, two-terminal devices are categorized in terms of transit time effect and bulk negative resistance effects. Two-terminal transit time effect devices are dominated by the impact avalanche transit time (IMPATT) device diode in their category, whereas the Gunn diode is the dominant one in bulk negative resistance effect devices. The IMPATT diode is regarded as the premier solid state device among their family. Similarly, the Gunn diode is regarded as the premier solid state device among devices which belong to the transfer electron effect family operating in sub-mm-wave and THz frequencies. Both of these categorized devices have been widely used in various communication systems as signal generators in recent years[1−6]. Thus the last decade has witnessed intense research activity, both theoretical and experimental, in the development of IMPATT and Gunn devices and associated systems for stable and reliable RF communication in the mm-wave range. Further, the materials used to fabricate such devices have also played a major role for high frequency operation in recent years. The materials used for this purpose in the last decade include mainly Si, GaAs, and InP. However, recently, high band gap semiconductors such as GaN and SiC have played a major role in high frequency high power generation[7−10]. With increasing maturity in epitaxial growth and improvement in crystal growth, III–V nitrides offer a high potential for high power microwave applications such as amplification and signal generation. High power GaN FETs and MODFETs have, for example, been reported with excellent electrical characteristics[2, 3]. However, very few theoretical as well as experimental results are available on GaN-based Gunn and IMPATT devices (to the author's knowledge)[11−14]. Therefore, authors feel the need to explore GaN based two terminal devices, namely IMPATT and Gunn diodes to provide a comparison to see the potential of each device using GaN material. For this, the authors have developed/modified their simulation software, which they normally use for traditional Si, GaAs based devices[15−18], and the results obtained from these studies are presented in this paper. This work will definitely be helpful to evaluate the potential of devices based on GaN material before significant resources are dedicated to material growth, device fabrication and characterization. A detailed formulation method for wide band gap semiconductor based transfer electron devices and avalanche transit time devices to study the static and dynamic characteristics is described. The results are summarized and presented with detailed comparisons. It is seen from our study that GaN-based IMPATTs produce ten times more power than a GaN-based Gunn diode, and the efficiency is far higher in IMPATT devices as compared to a Gunn diode. It may be mentioned here that there are two important forms of GaN materials used for such kind of devices. They are (Zincblende) Znb and (Wurtzite) Wz structures. Out of this two, Znb has better electrical characteristics than Wz and hence we have concentrated our study on a device based on a Znb structure only.

2. Methods developed for IMPATT and GUNN diodes

A novel method has been developed for the study of GaN-based IMPATT diodes and Gunn diodes and is presented in this section.

2.1. Model for GaN-based IMPATT devices

The IMPATT devices were designed following an IMPATT/MITATT mode DC simulation scheme which solves

* Project supported by the Department of Science and Technology, Government of India through SERC, FIST and TIFAC Program. The second author acknowledges the Regular Associate Award of ICTP, Trieste, Italy.
† Corresponding author. Email: akpanda62@hotmail.com
Received 28 October 2011, revised manuscript received 15 December 2011

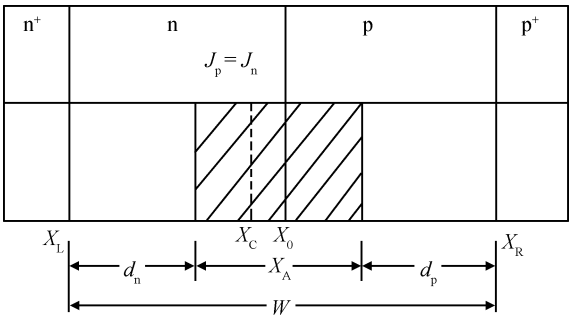

Fig. 1. Sketch of one dimensional model of an IMPATT diode structure, where x_0 is position of field maximum, x_c is position of avalanche centre ($J_p = J_n$); W is total active layer width, $d_{n,p}$ is widths of electrons and holes drift regions; x_A is avalanche zone width, x_L is left edge of the depletion layer, x_R is right edge of the depletion layer.

Poisson's equation:

$$\frac{\partial E}{\partial x} = \frac{q}{\varepsilon}(N_D - N_A + p - n). \tag{1}$$

Carrier continuity equations:

$$\frac{\partial n}{\partial t} = \frac{1}{q}\frac{\partial J_n}{\partial x} + g, \tag{2}$$

$$\frac{\partial p}{\partial t} = -\frac{1}{q}\frac{\partial J_p}{\partial x} + g, \tag{3}$$

where g is the carrier generation rate and includes avalanche and tunnel generation rate[4], and $J_{p,n}$ is current density, which includes drift, diffusion and tunnel current components and the mobile space charge equations:

$$q\frac{\partial(p-n)}{\partial x} = -q(\alpha_n - \alpha_p)(p-n) + J\left(\frac{\alpha_n}{\upsilon_p} + \frac{\alpha_p}{\upsilon_n}\right) + \frac{\partial E}{\partial x}K, \tag{4}$$

where K is a correction factor, whose value depends on the nature of the velocity-field characteristics in a semiconductor simultaneously with the standard boundary conditions. A brief summary of the structure is represented as a schematic diagram in Fig. 1. A double iterative computer program on the electric field maximum and position of the maximum electric field is developed and the above mentioned equations are solved simultaneously and consistently.

Our field extremum initiated computer method for DC analysis of IMPATT diodes is free from the numerical instability that is usually experienced in computer programs initiated from the edges of the depletion layer. The avalanche layer width of the diode is obtained as $X_A = |x_R + x_L|$. The edges of the avalanche region x_n and x_p can be determined from the condition of 95% multiplication position[4]. The drift zone is then given as $(W - x_n)$. The voltage drop across the different zones and avalanche zone is obtained by integrating the electric field over the respective zones. The diode breakdown voltage V_B is the sum of the avalanche voltage drop V_A and the drift zone voltage drop V_D. The approximate diode efficiency $\eta = \frac{V_D}{\pi V_B}$ can also be calculated from this DC analysis[7]. The output and final solution of this DC scheme is used as the input for our small-signal analysis of the IMPATT diode. A generalized method of analysis for high frequency characterization of an IMPATT diode, incorporating drift, diffusion and tunnel current is developed. Inclusion of drift, diffusion and tunnel current and solving the same for small signal analysis leads to a fourth-order differential equations on diode impedance[16].

$$\begin{aligned}&\Big(-D_A D^4 + \bar{D}D^3 + (1 + D_+ k - \bar{\alpha}_D)D^2 \\ &\quad + \Big\{\alpha_n - \alpha_p + 2rk - \frac{q}{\upsilon\varepsilon}D - \big[g'_T(x) + g'_T(x')\big]\Big\}D \\ &\quad + (2\bar{\alpha}k - k^2) + (\alpha'_n - \alpha'_p)DE_m - \bar{\alpha}'_D D^2 E_m - \frac{1}{\upsilon\varepsilon}2\bar{\alpha}'J \\ &- \frac{qr_p}{\bar{\upsilon}\varepsilon}\big[g'_T(x) + g'_T(x')\big] - \frac{q}{\bar{\upsilon}\varepsilon}D_- C_1(x)\Big)Z = \frac{1}{\bar{\upsilon}\varepsilon}(2\bar{\alpha} - k).\end{aligned} \tag{5}$$

The meanings of the parameters are described elsewhere, such as in Ref. [16].

This fourth-order differential equation has to be solved using the two available standard boundary conditions[16]. Therefore, a perturbation technique on diode impedance is used to solve Eq. (5). This technique leads to a series of second-order equations on diode impedance, which were solved simultaneously by a modified Runge–Kutta method within the active layer of the diode with the available boundary conditions and finally gives diode resistance $R = R_0 + \sum_K R_K$ and $X = X_0 + \sum_K X_K$, where R_0 and X_0 are unperturbed resistance and reactance whereas R_K and X_K are perturbed resistance and reactance which is due to diffusion of the charge carriers. Thus our method gives very accurate result including drift, diffusion and tunnel current. Further, integration of R and X, which are obtained at each space point, gives a diode total resistance Z_R and a diode total reactance Z_X. The device conductance G, device susceptance B are calculated respectively using the relations:

$$G = \frac{Z_R}{Z_R^2 + Z_X^2}, \quad B = \frac{Z_X}{Z_R^2 + Z_X^2}. \tag{6}$$

The small-signal analysis is repeated for several frequencies and the optimum frequency f_p corresponding to diode peak negative conductance ($-G_P$) is determined in each case. The diode negative resistance at $f_p(-Z_{Rp})$ and total diode negative reactance $-Z_X$ at f_p can also be determined from this analysis. Small signal power density $P_{RF} = \frac{V_{rf}^2}{2}G$ where V_{rf} represents the RF voltage swing considered as half the breakdown voltage in our case with 50% modulation is also computed from our simulation scheme. The microwave parameters computed in this way are used for the analysis of the IMPATT diodes by incorporating realistic variations of drift velocity (v_d), ionization of the charge carriers and all other material parameters, which are summarized and represented in Refs. [4, 16].

2.2. Models for GaN-based GUNN diode

We have developed a versatile and explicit numerical technique based on the first principle approach of the device, which accurately predicts the device characteristics and agrees well with the experimental values measured for operating devices for a Gunn diode. A one-dimensional model as shown in Fig. 2

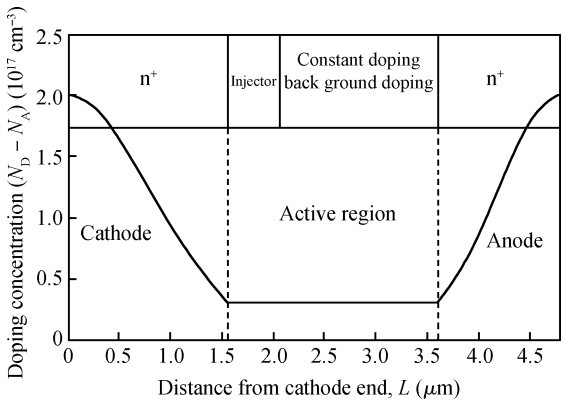

Fig. 2. Typical structure and doping profile of a GaN/AlGaN type Gunn diode.

is considered to study the domain dynamics in the device because the domain propagation occurs between the parallel contacts, and because the length of the uniformly doped active n-layer is typically much smaller than the device diameter. The structural model used in the computer simulation is shown in Fig. 2. The simulation of solid state devices requires the solution of a transport equation that describes the carrier response to the fields, and Poisson's equation, which describes the evolution of the field due to the carrier movement. A finite difference numerical method is developed to solve the carrier continuity equation, Poisson's equation, and the space charge equation with a realistic velocity-field characteristic in the device (like that of IMPATTs)[16]. The field dependent diffusion is also taken into consideration.

In addition to Poisson's equation and the carrier continuity equation, the complete device simulation requires the specification of boundary conditions. These can be either voltage or current boundary conditions. Voltage boundary conditions are used in this model, which requires the integral of the electric field across the device to be equal to the applied voltage. Other conditions such as the device contacts being ohmic and the total current density to be continuous throughout the device are also taken into consideration. The electric field boundary conditions at the outer metal contact edges of the n^+ region (anode and cathode ends) are taken to be zero. Thus the time dependence of the electric field at the two edges of the active region is removed. The limits on the space step (Δx) and time step (Δt) are derived from simple physical considerations. In summary, the device simulation consists of:

(1) Updating the electric field at the future time step by solving Poisson's equation and satisfying the condition $V^{t+\Delta t} = -\int_0^L E\mathrm{d}x$, where $V^{t+\Delta t}$ is the terminal voltage at $t + \Delta t$ and L is the device length.

(2) Computing the electron mobility from the velocity-field characteristics and the diffusion coefficient from Einstein's relation at every space step.

(3) Solving the current continuity equation for the carrier concentration at the future time step.

(4) If the simulation time is not reached, repeat all above again from step (1).

The presence of Gunn domains leads to fluctuations of voltage and current, which gradually built-up into sustained large-signal oscillations. These voltage $V(t)$ and current $I(t)$ waveforms, corresponding to sustained oscillations, were subjected to harmonic analysis and the resulting power spectrum was used to determine the frequency and power of the Gunn diode oscillators. The details are described below.

The fluctuations in terminal voltage can be represented as:

$$V(t) = V_{\mathrm{dc}} + V_{\mathrm{rf}}\,\mathrm{Sin}(\omega t). \tag{7}$$

The current density across the device is expressed as:

$$J_{\mathrm{T}}(x,t) = qn(x,t)v(x,t) + \varepsilon\frac{\partial E(x,t)}{\partial t}. \tag{8}$$

Integrating Eq. (8) over the length of the device results in:

$$\int_0^w J_{\mathrm{T}}(x,t)\mathrm{d}x = \int_0^w qn(x,t)v(x,t)\mathrm{d}x + \frac{\varepsilon}{W}\int_0^w \frac{\partial E(x,t)}{\partial t}\mathrm{d}x. \tag{9}$$

The first term on the right-hand side corresponds to the average particle current density $J_{\mathrm{p}}(t)$ and the second term to the displacement current density. For the purpose of determining device performance, it is only necessary to consider the first term. The second term through the device's cold capacitance can then be added to the equivalent circuit if necessary. The resulting particle current density can be Fourier analyzed to extract the DC and the fundamental components as follows. The particle current density $J_{\mathrm{p}}(t)$ can be written as $J_{\mathrm{p}}(t) = J_{\mathrm{dc}} + J_{\mathrm{rf}}(t)$, where

$$J_{\mathrm{dc}} = \frac{1}{T}\int_0^T J_{\mathrm{p}}(t)\mathrm{d}t, \tag{10}$$

$$J_{\mathrm{rf}}(t) = a_1\cos(\omega t) + b_1\sin(\omega t). \tag{11}$$

Fourier components a_1 and b_1 can be written as:

$$a_1 = \frac{2}{T}\int_0^T J_{\mathrm{p}}(t)\cos(\omega t)\mathrm{d}t, \tag{12}$$

$$b_1 = \frac{2}{T}\int_0^T J_{\mathrm{p}}(t)\sin(\omega t)\mathrm{d}t. \tag{13}$$

The device admittance per unit area is given as:

$$Y_{\mathrm{D}} = -G_{\mathrm{D}} + \mathrm{j}B_{\mathrm{D}}, \tag{14}$$

where

$$G_{\mathrm{D}} = \frac{b_1}{V_{\mathrm{rf}}}, \tag{15}$$

and

$$B_{\mathrm{D}} = \frac{a_1}{V_{\mathrm{rf}}} + \frac{\omega\varepsilon}{W}. \tag{16}$$

The generated RF power is given by

$$P_{\mathrm{rf}} = \frac{1}{2}V_{\mathrm{rf}}^2 AG_{\mathrm{D}}, \tag{17}$$

where A is the device area. From here, the DC to RF conversion efficiency can be calculated as $\frac{P_{\mathrm{rf}}}{P_{\mathrm{dc}}}$, where $P_{\mathrm{dc}} = V_{\mathrm{dc}}I_{\mathrm{dc}}$. I_{dc} can be calculated from Eq. (10). Thus the power obtained and

Table 1. Optimized design parameters for the GaN-based Gunn diode.

Structure	Length of the anode, L_a	Length of the cathode, L_c	Length of the active region	Background doping concentration	Active region doping, n	Biasing DC value	Doping of anode and cathode region
Str1	1.2 μm	0.8 μm	5 μm	10^{13} cm^{-3}	10^{16} cm^{-3}	90 V	10^{19} cm^{-3}

Table 2. Optimized structural parameters for the GaN-based IMPATT diode.

Structure	Width (μm)		Doping (10^{17} cm^{-3})	
	n-side	p-side	n-side	p-side
Znb GaN n$^+$npp$^+$ DDR	0.530	0.265	2.95	5.80
Wz GaN n$^+$npp$^+$ DDR	0.530	0.265	2.95	5.80

Table 3. Device properties for different DDR IMPATT.

Structure	Wz n$^+$npp$^+$	Znb n$^+$npp$^+$
E_{peak} (MV/cm)	4.54	3.21
V_B (V)	165.22	95.77
η (%)	12.5	11.4
Power density (10^7 W/cm^2)	2.48	2.78

Table 4. Device properties of the Gunn diode at different bias voltages.

Bias voltage	70 V	80 V	90 V	100 V
η (%)	2.5	3.21	2.84	0.43
Power density (10^7 W/cm^2)	0.078	1.21	1.40	0.0198

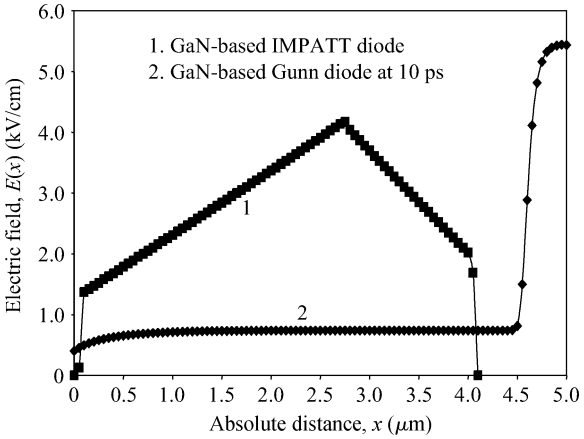

Fig. 3. Electric field formations from cathode end to anode end for the Gunn diode at 10 ps and electric field for the IMPATT diode from the p-end at its optimized structure.

DC to RF conversion efficiency for any type of Gunn diode including hetero-structures can also be computed from our simulation program. All the realistic material parameters are also used in this case. The developed method is validated with the available experimental as well as theoretical results obtained earlier for both Gunn[5, 17] and IMPATT diodes[16, 18] for traditional Si and GaAs-based devices and is expected to work for GaN-based devices too at this operating frequency region. We have used the standard design criterion for both IMPATTs and Gunn diodes described elsewhere[5, 16]. The computed results using the above described methods are analyzed and compared in the next section for IMPATT and Gunn diodes.

3. Comparative results and discussion

Simple schematic diagrams for Gunn and IMPATT diodes are shown in Figs. 1 and 2, respectively. Initially, the diode structures (for both Gunn and IMPATT), doping profiles, current density, bias voltage etc are optimized for the same operating conditions keeping it in mind to operate at 94 GHz for both IMPATT and Gunn diodes using the same procedure as described in Refs. [7, 17]. This is done by using our previous techniques [7, 17]. The optimized structures are presented in Tables 1 and 2 for Gunn and IMPATT diodes, respectively. The diodes were simulated using these structures. DC and high frequency characteristics were determined for both the polytypes of GaN-based IMPATTs and some of the results are presented in Table 3. Whereas the characteristics were determined for a Znb-based Gunn diode at various bias voltages and are presented in Table 4. It is mentioned here that earlier it was shown that Znb-based GaN IMPATTs give better microwave properties and have better v–E characteristics than Wz-based GaN. Since then, Gunn diodes have provided better microwave properties from the materials having better v–E characteristics and Znb GaN IMPATTs produce better properties, we have considered Znb-GaN for comparison purposes.

The maximum electric field obtained in the device represents indirectly the velocity at which the carriers are moving. High electric field brings the velocity of the carriers into the saturation region and determines the maximum operating frequency in case of IMPATTs. Similarly integration of the electric field profile gives the diode breakdown voltage and that represents the maximum power generated by the device[7, 18]. Similarly, a high electric field at the cathode end bring the carriers into saturation, domain forms quickly and decides the oscillation frequency[12] as well as power generated in case of the Gunn diode. Therefore, electric field curves at a particular instant are drawn in Fig. 3 for the Gunn and IMPATT diodes, and the maximum electric field is represented in Tables 3 and 4. It is seen from Table 3 that the maximum electric field at the junction (E_{peak}) is 3.21 $\times$ 10^6 V/cm and the diode breakdown voltage (V_B) is found to be 95.77 V for Znb structure IMPATT devices which will be compared with the Znb structure Gunn diode. Table 3 also represents the efficiency. From Table 3, it is seen that efficiency (η) is 11.4% for the IMPATT device, where it is only 3.21% for Gunn diode (Table 4) at optimized

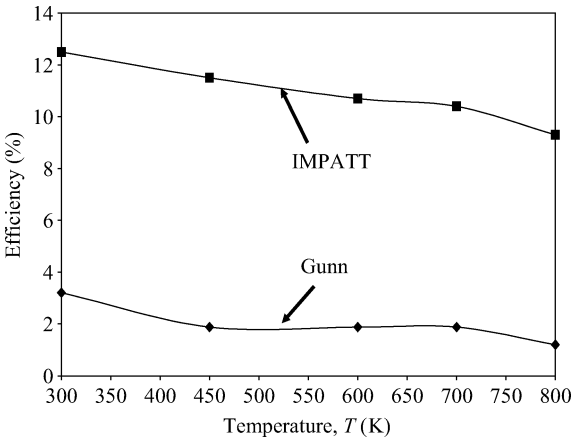

Fig. 4. Efficiency comparison of Gunn and IMPATT diodes at different temperatures.

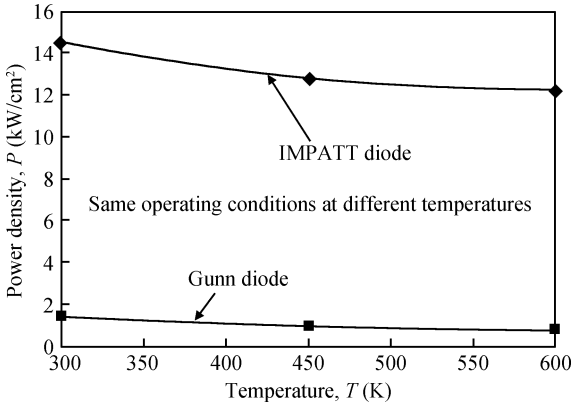

Fig. 5. Power density at different temperatures for Gunn and IMPATT diodes.

bias voltage. The method of determination of efficiency for the Gunn diode is as described in Section 2 and Ref. [5]. Thus, to analyze the characteristics of Gunn and IMPATT diodes, the electric field curves at different positions (for IMPATT from the p-end and for Gunn from the cathode end) are drawn and are shown in Fig. 3. The electric field drawn for the Gunn diode is captured at 10 ps simulation time (to have the operating frequency of 94 GHz). Figure 3 shows that the maximum electric field obtained from IMPATT diode is around 4.5 kV/cm. However, the electric field at this time is higher in the Gunn diode at the anode end only. In the Gunn diode, the electric field remains almost constant throughout the active region and thus the integrated bias voltage is less than that of the IMPATT diode leading to higher power generation from the IMPATT than the Gunn diode.

Further, using our simulation scheme, the power generated from such devices is also determined. A power density (represented in Tables 3 and 4) of 2.78×10^7 W/cm^2 is generated from Znb GaN-based IMPATT devices. For the same kind of structure with a Gunn diode, the power generated is around 1.40×10^7 W/cm^2. As mentioned, the integration of electric field determines the breakdown voltage and determines the efficiency of the IMPATT diode whereas the DC component in the current density curves obtained determines the efficiency of the Gunn diode. Thus efficiency is determined for both the cases and a comparative figure is drawn and shown in Fig. 4 at different temperatures keeping all other operating conditions the same. It is seen from the figure that efficiency in both cases remains almost constant at different temperatures showing the stability of GaN-based diodes. However, the same figure shows that efficiency is at least three times more in the GaN-based IMPATT diode compared to the Gunn diode at this operating frequency. This shows that IMPATT diodes have better efficiency than Gunn diodes. To provide further proof about the credibility of IMPATT diodes, the power density is also determined for both of the diodes at different temperatures (at optimum frequency) using the same technique as described in Section 2. The peak power density at optimum frequency of operation at different temperatures is drawn in Fig. 5 for both the diodes. It is seen from the figure that the power is found to be 1.48×10^7 W/cm^2 for GaN-based IMPATT diodes, clearly indicating that the power obtained from GaN-based IMPATT diodes will be almost ten times more than that of GaN-based Gunn diodes. Also, it is seen from the figure that with increase in temperature, the frequency of operation remains the same in all these cases unlike that of traditional GaAs-based devices where with increase in temperature, the operating frequency shift towards higher value[4]. In GaN cases, though the power generated decreases slightly with increase in temperature, the dynamic properties remain the same for temperature up to 600 K. This indicates that GaN-based Gunn diodes and IMPATT diodes can be operated at higher temperature. However, at high temperatures the power obtained from a GaN-based Gunn diode is less than that of a GaN-based IMPATT diode; indicating clearly that GaN-based IMPATT diodes have advantages over GaN-based Gunn diodes.

4. Conclusion

Simulation studies of GaN-based Gunn and IMPATT diodes are presented. A novel method has been developed for both the cases. All possible types of structural variations of the diodes are considered to explore the possibility of improving performance. The RF power and efficiency obtained from GaN-based IMPATT devices is expected to be very high as compared to a GaN-based Gunn diode. The dynamic properties of GaN-based Gunn diodes remain almost same for temperatures up to 600 K. This indicates that GaN-based diodes can be operated at high temperature. However at high temperature, the power obtained from a GaN–based Gunn diode is less than that of GaN–based IMPATT diodes. A 2 to 10 times higher power output for GaN-based IMPATT diodes compared to the GaN-based Gunn diode is noteworthy. From our study, it may be concluded that a GaN-based IMAPTT diode is expected to generate higher power at high frequency compared to a Gunn diode and these data can be used as first-hand information by experimentalists.

References

[1] Yang L, Hao Y, Yao Q, et al. Improved negative differential mobility model of GaN and AlGaN for a terahertz Gunn diode. IEEE Trans Electron Devices, 2011, 58(4): 1076

[2] Heller E R, Ventury R, Green D S. Development of a versatile physics-based finite-element model of an AlGaN/GaN HEMT capable of accommodating process and epitaxy variations and calibrated using multiple DC parameters. IEEE Trans Electron Devices, 2011, 58(4): 1091
[3] Lenka T R, Panda A K. Characteristics study of 2DEG transport properties of AlGaN/GaN and AlGaAs/GaAs-based HEMT. Semiconductors, 2011, 45(5): 650
[4] Panda A K, Pavlidis D, Alekseev E. Noise characteristics of GaN-based IMPATTs. IEEE Trans Electron Devices, 2001, 48(7): 1473
[5] Panda A K, Dash G N, Agrawal N C, et al. Studies on the characteristics of GaN-based Gunn diode for THz signal generation. IEEE APMC, 2009: 1565
[6] Sze S M. Modern semiconductor device physics. New York: John Wiley and Sons, 1998
[7] Panda A K, Parida R K, Agrawala N C, et al. Comparative study on the high-bandgap material (GaN and SiC)-based impact avalanche transit time device. IET Microwave, Antenna and Propagation, 2008, 2(8): 789
[8] Mukherjee M, Mazumder N, Roy S K. Photosensitivity analysis of gallium nitride and silicon carbide terahertz IMPATT oscillators: comparison of theoretical reliability and study on experimental feasibility. IEEE Trans Device Mater Reliab, 2008, 8(3): 608
[9] Yang L, Hao Y, Zhang J. Use of AlGaN in the notch region of GaN Gunn diodes. Appl Phys Lett, 2009, 95(14): 143507
[10] Barry E A, Sokolov V N, Kim K W, et al. Large-signal analysis of terahertz generation in submicrometer GaN diodes. IEEE Sensors Journal, 2010, 10(3): 765
[11] Alekseev E, Pavlidis D. Large-signal microwave performance of GaN-based NDR diode oscillators. Solid-State Electron, 2000, 44(6): 941
[12] Khalid A, Li C, Dunn G, et al. Observation of multiple domains in a planar Gunn diodes. Proceedings of 4th European Microwave Integrated Circuits Conference, Rome, 2009: 298
[13] Mukherjee M, Mazumder N, Roy S K. Photosensitivity analysis of gallium nitride and silicon carbide terahertz IMPATT oscillators: comparison of theoretical reliability and study on experimental feasibility. IEEE Trans Device Mater Reliab, 2008, 8(3): 608
[14] Mukherjee M. Hexagonal GaN based photo-irradiated IMPATT devices for application in MM-wave communication systems. International Conference on Emerging Trends in Electronic and Photonic Devices and Systems, 2009: 483
[15] Mukherjee M, Roy S K. Optically modulated III–V nitride-based top-mounted and flip-chip IMPATT oscillators at terahertz regime: studies on the shift of avalanche transit time phase delay due to photogenerated carriers. IEEE Trans Electron Devices, 2009, 56(7): 1411
[16] Panda A K, Dash G N, Pati S P. Computer-aided studies on the wide-band microwave characteristics of a silicon double avalanche region (DAR) diode. Semicond Sci Technol, 1995, 10(6): 854
[17] Panda A K, Agrawal N C, Parida R K, et al. GaN-based gunn diode for high frequency signal generation. International Workshop on Physics of Semiconductor Devices, 2007: 514
[18] Agrawala N C, Parida R K, Dash G N, et al. Optimised implantation profiles for the p–n junction using fourth moment approach for application in high frequency VLSI circuits. Transaction in Electronics, Electrical and Communication Engineering, 2008, 6(2): 44